In-situ soot characterization of propane flames and influence of additives in a 100 kW oxy-fuel furnace using two-dimensional laser-induced

Available online at www.sciencedirect.com

ScienceDirect

Proceedings of the Combustion Institute 37 (2019) 833–840

Proceedings of the Combustion Institute

www.elsevier.com/locate/proci

In-situ soot characterization of propane flames and influence of additives in a 100 kW oxy-fuel furnace using two-dimensional laser-induced incandescence

J. Simonsson [a,*], A. Gunnarsson [b], M. Naduvil Mannazhi [a], D. Bäckström [b], K. Andersson [b], P.-E. Bengtsson [a]

[a] *Division of Combustion Physics, Lund University, Lund, Sweden*
[b] *Division of Energy Technology, Chalmers University of Technology, Gothenburg, Sweden*

Received 29 November 2017; accepted 6 May 2018
Available online 22 June 2018

Abstract

In-situ soot characterization has been successfully performed in a 100 kW_{th} down-fired oxy-fuel test furnace using laser-induced incandescence (LII) and extinction measurements. Primarily non-premixed propane flames were investigated in oxy-fuel mode with various concentrations of oxygen in the oxidant. The turbulent flame character was manifested through two-dimensional single-shot LII signals from soot showing strong spatial variations as well as local temporal variations. The LII signals were calibrated to soot volume fractions, f_v, using in-situ extinction in the same spatial regions of the furnace. The results show increased f_v for increasing oxygen concentration in the oxidant, which is related to increased temperatures as well as decreased mixing inside the furnace due to lowered total flow. For some measurement cases, the influence of additives was studied for flames in oxy-fuel and air environments. The results showed increased f_v for additions of SO_2 and NO for oxy-fuel conditions, while a decrease of f_v was found for air-fed flames. Also, a large decrease in f_v was found for water injection in the air-fed flames, and a slightly larger decrease for addition of KCl dissolved in water with the same amount of injected solution. Uncertainties in performing soot volume fraction measurements using LII and extinction in this large-scale furnace are discussed, and mainly considered to be uncertainties in $E(m)$ for soot, the spatial variation of the laser fluence in the large imaged area, and the estimation of the absorption length during extinction calibration.

Keywords: Oxy-fuel; Laser-induced incandescence; Soot; Potassium; Extinction

Introduction

Oxy-fuel combustion is a fuel conversion technology for which CO_2 emissions, in combination with storage, could be eliminated, and hence of great interest in order to restrict global

* Corresponding author.
E-mail address: johan.simonsson@forbrf.lth.se (J. Simonsson).

https://doi.org/10.1016/j.proci.2018.05.035

warming. In furnaces using such technology, knowledge of soot formation processes is important as strong radiative heat transfer results from high soot concentrations. However, soot in the exhaust of such applications must be minimized as soot is negative for environment [1] as well as health [2]. Also, recent studies have shown that soot is one of the major contributors to global warming together with carbon dioxide and methane [1,3].

Knowledge of radiative heat transfer in furnaces is crucial, which motivates development of more accurate heat transfer models to improve these devices. This requires knowledge about multiple parameters, e.g. temperature, gas composition, and particle concentration. These parameters can favorably be studied in a controlled test facility of reasonable size. At Chalmers University of Technology, Gothenburg, Sweden, a 100 kW_{th} test furnace, capable of running both gaseous and solid fuels in oxy-fuel and air environments, is located. Flames in both oxy-fuel and air environments have been investigated in this facility using various techniques, see e.g. [4–6]. Most of the studies have utilized probes for radiative measurements inside the furnace and gas extraction for further analysis by external measurements. Andersson et al. [7,8] measured temperature, gas composition, and total radiative intensity using propane and lignite as fuels. A discrete transfer model was used for calculation of the total radiative intensity, and it was shown that the measured intensity levels could not be reached without taking radiation from soot into account. In [9], Mehta et al. presented results showing that soot particles could contribute up to 70% of the total emitted flame radiation. In a recent study [10], Bäckström et al. sampled gas at different locations inside the furnace to locally evaluate particle sizes and soot volume fractions using a Scanning Mobility Particle Sizer. For the flames investigated in [10], the radiative intensity was measured and modeled using experimentally measured soot volume fractions as an input to the model, and the radiative intensity calculated from the model was found to be in good agreement with measured data.

Extractive techniques and probes in general suffer from several limitations since they only give highly localized spatial information, perturb the flow and flame conditions, and may also change the particle characteristics. Alternatively, optical techniques can be used, exemplified by measurements of the thermal radiation from flames from which temperatures and soot concentrations can be estimated. Optical techniques have a merit of being non-invasive, i.e. they do not perturb the combustion process. Still, a limitation of such radiation measurements is that the detected signals are line-of-sight averaged, i.e. the data is not spatially resolved along the direction of detection. Another limitation is that optical techniques require optical access, which sometimes can be hard to accomplish in large-scale devices.

During the last decades, laser techniques have been developed and applied to numerous practical combustion devices. They have been successful in providing two- or even three-dimensional data of various parameters. For soot detection, especially laser-induced incandescence (LII) [11,12] has been used for absolute soot concentration measurements. Since LII can provide temporally as well as spatially resolved soot concentrations, such data can lead to more fundamental understanding of the turbulent flame interactions and significant improvement of radiative heat transfer models. Previous applications of laser diagnostics to these types of furnaces are scarce and dominated by diode-laser absorption spectroscopy. These lasers can be tuned to specific transitions of molecules to retrieve species concentrations, however, only spatially averaged line-of-sight. A successful application of diode-laser absorption to oxy-fuel systems is for example [13], and measurements using LII in small-scale oxy-fuel flames can be found in [14].

In this work we present results from soot measurements performed in primarily oxy-fuel environments using laser-induced incandescence, where extinction measurements were used for absolute calibration of LII data. We observed strong increase in evaluated soot volume fraction for increasing oxygen concentrations in the oxidant based on averaged data, and analyzed the stochastic fluctuations from the temporally resolved 2-D data. The effects of additives of $KCl_{(aq)}$, H_2O, SO_2, and NO on the soot concentration were also studied for some operating conditions in both oxy-fuel and air environments. We also discuss the challenges we experienced when applying LII in this test furnace, as well as discuss uncertainties and limitations related to the measurements and calibration of two-dimensional LII images to soot volume fractions.

Experimental description and evaluation routine

In-situ soot measurements were performed using laser-induced incandescence (LII) [11,12] and extinction. LII is a technique where incident laser pulses are absorbed by soot particles, giving rise to an increased particle temperature and consequently to incandescence. This increased radiation above the normal flame luminosity is called the LII signal. The LII signal has been shown to be approximately proportional to soot volume fractions [15], but has to be calibrated to achieve quantitative data. Extinction measurements can be used for quantitative soot volume fraction measurements, and thereby utilized for calibration of LII. Extinction is a line-of-sight technique for which the decrease in light intensity through an absorbing medium with an absorption path length, L, is measured. In this work, the extinction coefficient, K_{ext}, was extracted from

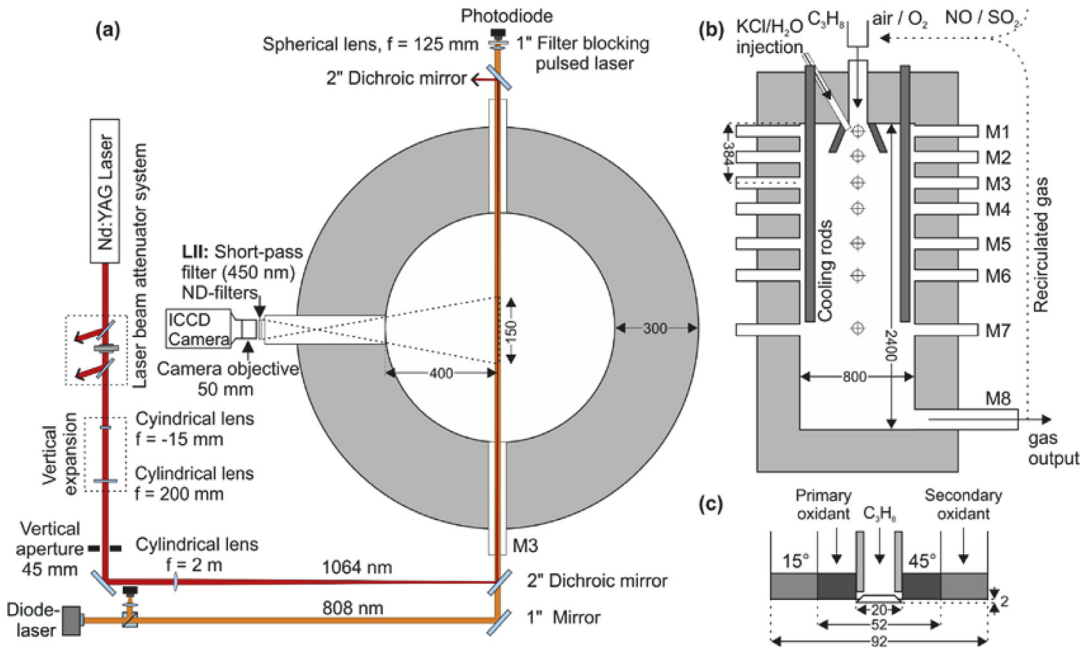

Fig. 1. Illustrations of (a) the optical setup, (b) the furnace, and (c) the fuel and oxidant registers. All lengths are in mm unless otherwise stated. The measurement ports are called M1 to M8.

Beer-Lamberts law, $I = I_0 e^{-K_{ext} L}$, knowing the initial intensity, I_0, and the transmitted intensity, I. By assuming that the soot particles are spherical and that the measurements take place within the Rayleigh limit, i.e. the particles are much smaller than the used wavelength, it is common to neglect the scattering as part of the extinction [16]. These assumptions are discussed in for example [17]. Under these assumptions, the soot volume fractions, f_v, can be calculated using:

$$f_v = \frac{K_{ext}\,\lambda}{6\pi\,E(m)} \quad (1)$$

where λ represents the laser wavelength and $E(m)$ is the absorption function, often calculated from the complex refractive index, m, using $E(m) = -\mathrm{Im}((m^2 - 1)/(m^2 + 2))$.

The combined LII and extinction setup is presented in Fig. 1a together with a schematic image of the furnace in Fig. 1b, and a detailed image of the fuel and air registers in Fig. 1c. The measurements were performed on an 80 kW propane flame in Chalmers 100 kW_{th} oxy-fuel test furnace, and all measurements were performed in measurement port M3, with its center located 384 mm from the top of the furnace. The furnace can be operated with air, oxygen-enriched air, as well as in oxy-fuel mode by recirculating a portion of the dry flue gas consisting mainly of carbon dioxide and excess oxygen. Hence in oxy-fuel mode, the oxidant consists of carbon dioxide and oxygen in varying amounts, see Table 1. It should be noted that increasing oxygen concentration in the oxidant correlates with less carbon dioxide recirculated to the furnace and by a lower total oxidant flow. The fuel and the oxidants are introduced in the top-center of the furnace where the oxidant (including recirculated gas) enters through two swirling registers, with angles of 15 and 45 degrees. The flow through the registers could be controlled by opening or closing of valves connected to each register. For all test cases, the flow of propane was constant at 1.73 g/s and the oxygen-to-fuel equivalence ratio, also often referred to as the air-to-fuel equivalence ratio, λ, was set to be constant at 1.15, i.e. slightly lean overall.

The LII setup consists of two main components; an Nd:YAG laser operating at the fundamental wavelength, 1064 nm, and an ICCD-camera for detecting the LII signal. The laser beam was shaped to a 4.5 cm high Gaussian sheet focused in the center of the furnace using a cylindrical lens with focal length of two meter. The long focal length was used to get a longer beam waist and more uniform laser fluence over the imaged two-dimensional region. At flame center, a laser fluence of 0.8 J/cm^2 was used, which is on the so-called fluence plateau [18] where the LII signal is rather insensitive to variations in laser intensity. This is beneficial for the use of LII in practical applications, to avoid uncertainties arising from laser energy absorption by soot. The ICCD-camera was placed orthogonally to the laser beam. A short-pass filter with a cut-off wavelength at 450 nm was placed in front

Table 1
The operating conditions used for the different test cases. For the oxy-fuel cases the fraction that is not oxygen is mainly carbon dioxide.

	Test case	Oxygen in oxidant [%]	Oxidant flow [Nm^3/h]	Primary oxidant register	Overall oxygen-to-fuel equivalence ratio, λ
Oxy-fuel	1	25	73.0	Open	1.15
	2	30	60.8	Open	1.15
	3	35	52.1	Open	1.15
	4	40	45.6	Open	1.15
	5	42	43.4	Open	1.15
Air	6	21	86.9	Open	1.15
	7	21	86.9	Closed	1.15

of the camera to suppress the major part of the background luminosity of the flame. In addition to the short-pass filter, neutral density filters were also placed in front of the camera to avoid saturation at the conditions giving the highest signals. For every measurement case, at least 500 single-shot images were recorded with a camera gate width of 50 ns. A background luminosity image was recorded 5 μs before each laser pulse and has been subtracted from each LII image. In the resulting LII images the size of one pixel corresponds to a length of 420 μm inside the flame. For further discussion regarding the LII setup, see for example [19,20].

The extinction measurements were conducted using a diode laser modulated on and off with a frequency of 250 Hz to be able to measure a background signal between each laser pulse. The laser was operated at a relatively long wavelength of 808 nm to prevent absorption by polycyclic aromatic hydrocarbons (PAHs), as discussed in [17]. Based on previous measurements in the same facility, the scattering contribution to the extinction was estimated to be less than 3% for a flame corresponding to case 7 [10,21]. To accomplish valid quantitative calibration, the laser beam with a diameter of approximately 5 mm was overlapped with part of the laser sheet from the Nd:YAG laser. For more information regarding the setup used for the extinction measurements, see for example [17].

The calibration procedure can be described in four steps: **(1)** An average of the LII signal was evaluated at the spatial position where the 808 nm extinction laser overlaps with the LII laser (approximately 21 mm from the top edge of the LII laser), see Fig. 2a. A vertical average (± 2 mm) in the LII image resulting in a horizontal cross section will be used for step 2, and an average of the entire dashed area will be used for step 4. **(2)** Evaluation of the absorption length was made in order to calculate the soot volume fraction averaged along the extinction laser path. For most cases, the averaged LII images were used to estimate the absorption length, see Fig. 2b. This procedure was not possible for case 5 (see Table 1) since the LII signal extended outside the observable region for the CCD detector, and the absorption length was assumed to be

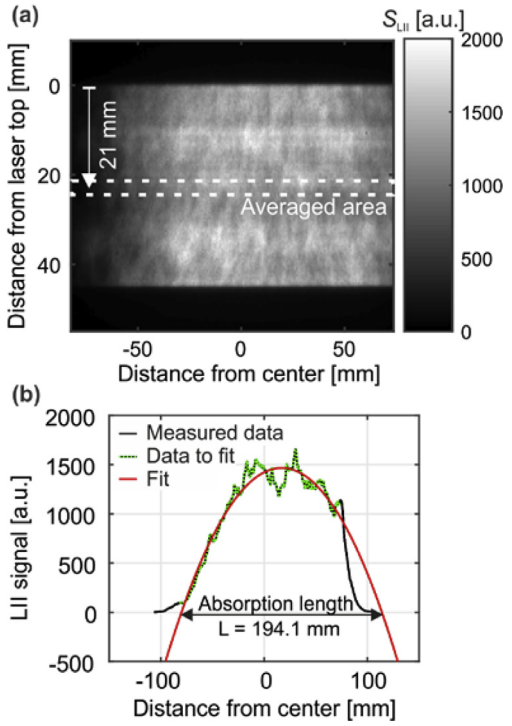

Fig. 2. (a) presents the first step of the calibration procedure, i.e. calculation of the average LII signal used in step 2 and for attaining the corresponding LII signal to the measured soot volume fraction. (b) shows the second step of the calibration procedure, where an estimation of the absorption length based on averaged LII signals are performed.

the entire inner diameter of the furnace, i.e. 0.8 m. **(3)** The soot volume fraction was then calculated using Beer-Lambert law and Eq. (1), and will yield soot concentrations averaged along the laser beam. **(4)** A ratio between the LII signal, averaged in step 1, and the soot volume fraction was calculated, and used to translate both single-shot images as well as averaged LII images to two-dimensional soot volume fraction images, since the LII signal

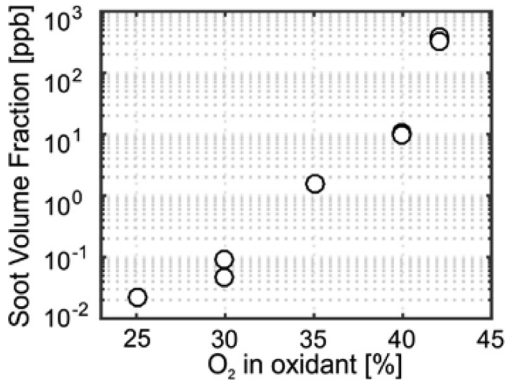

Fig. 3. Soot volume fractions as function of oxygen concentration in the oxidant for measurements in oxy-fuel environment, i.e. cases 1–5 in Table 1.

is approximately proportional to the soot volume fraction [15]. The LII-to-f_v ratio is valid for all cases provided that the LII signals have been measured using the same optical equipment, laser energy, and camera settings. The strength of this semi-simultaneous extinction calibration method in comparison with others is that the calibration is performed on soot at exactly the same location in the furnace.

3. Results and discussion

In Fig. 3, results from the measurements of LII calibrated using extinction measurements, are presented. The graph presents soot volume fractions as function of oxygen concentration in the oxidant for the oxy-fuel measurements. The LII signals have been averaged over the entire field-of-view at the level in the furnace where the extinction laser passed through. The absorption function, $E(m)$, used in the evaluation of soot volume fractions was set to 0.35, based on measurements conducted in our laboratory ethylene/air flames [22,23].

The results show a strong increase in soot volume fraction for increased oxygen concentration in the oxidant, although the overall oxygen-to-fuel equivalence ratio in the furnace remains constant ($\lambda = 1.15$) for all cases, as presented in Table 1. To achieve this, the flow of oxidant has to be decreased when increasing the oxygen level, since the flow of propane is constant at 1.73 g/s. The reduced total flow inside the furnace, causes a higher temperature as the recirculated CO_2-flow is reduced. It is well-known that increasing temperatures in non-premixed flames result in higher soot volume fractions [24]. Hence the strong increase of soot volume fraction for increasing oxygen concentrations may be a combined effect of increasing temperatures and reduced mixing of fuel and oxidant. Similar observations have been made by Shaddix and Williams in lab-scale measurement of non-premixed methane flames on a simplified geometry [14], i.e. that reduced soot concentration is associated with increased mixing and higher temperatures. Furthermore, measurements were also conducted using oxygen-enriched air under the same equivalence ratio as for the oxy-fuel measurements. Using oxygen-enriched air results in higher temperatures caused by a lower molar heat capacity for N_2 compared to CO_2 [24], which consequently led to soot volume fractions at the same level as for oxy-fuel with 42% O_2 already at 30% O_2 for the oxygen-enriched cases. This indicates a strong influence of temperature on the soot formation.

The results presented in Fig. 3 originate from averaging of two-dimensional single-shot images. In Fig. 4, two-dimensional images of soot are shown, one single-shot image from case 4 and averaged images of cases 4 and 5. Based on the single-shot image in Fig. 4a, it is clear that soot is formed very locally with clearly visible soot structures with local concentrations up to 1 ppm for this single shot of case 4. However, the averaged soot concentration presented in the first image of Fig. 4b is much lower (up to 33 ppb), which is expected as large portions of the imaged area in the single-shot images do not contain any soot, and the fact that the flames are turbulent. In Fig. 4c, single-shot statistics are shown for case 4, where the maximum soot volume fraction in a square of 10×10 pixels (corresponding to 4 mm x 4 mm in the furnace) is retrieved from each single-shot frame (in this case 1000 frames) and presented in a histogram with bin size of 20 ppb. The distribution was found to be highly skewed with 54% of the observations between 0 and 20 ppb, while few observations showed soot volume fractions up to around 1 ppm, which strengthens the earlier statement that the flame is highly turbulent. The images with high soot concentrations, case 5, in Fig. 4b, will be discussed later.

Various measurements were performed to study the influence of additives on soot formation, and the results are presented in Fig. 5. The potassium chloride (KCl) solution in H_2O and a reference with the same amount of H_2O were sprayed directly onto the flame through the angled probe port on top of the furnace, see Fig. 1b. The amount of $KCl_{(aq)}$ (1 M) or water sprayed was set to 0.15 ml/min, which is equivalent to ~100 ppm in the flue gas for a case with 21% O_2 under the assumption of complete combustion. The other additives, NO and SO_2, were introduced in the oxidant and carried through the different oxidant registers. The amount of SO_2 added to the flame was around 550 ppm in the oxidant. For NO, the amount of additive in the oxidant was set to approximately 0.7 Nl/min.

For the oxy-fuel cases 4 and 5, the results show an increase of the soot concentration when introducing either NO or SO_2, with somewhat larger

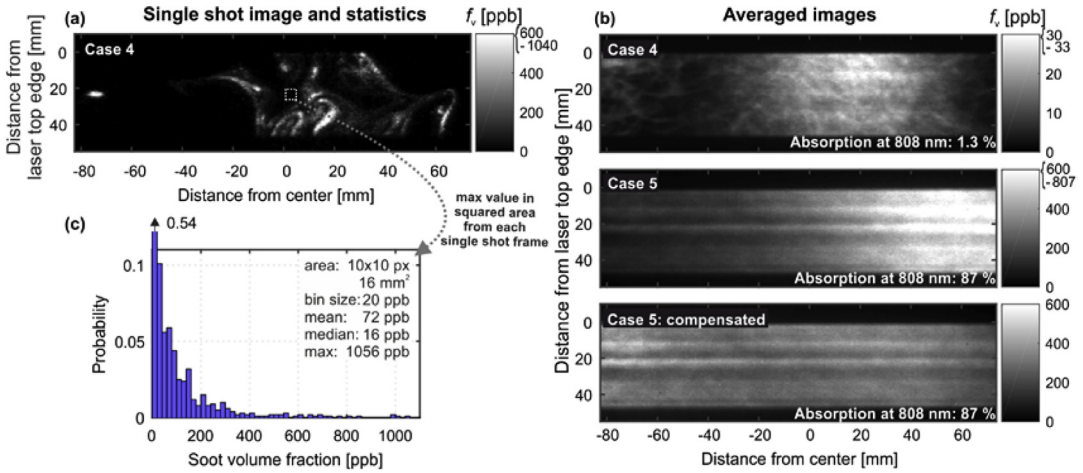

Fig. 4. (a) Single-shot image showing soot volume fractions for case 4. (b) Averaged images for cases 4 and 5 as well as an image for case 5 which has been compensated for windows fouling, absorption of the LII signal as well as absorption of the laser radiation. (c) Statistics of maximum soot volume fraction in defined square of 10×10 pixels for 1000 frames of case 4. To increase visibility in the 2D-images, the range of the images has been limited, i.e. the color white corresponds to a range of values.

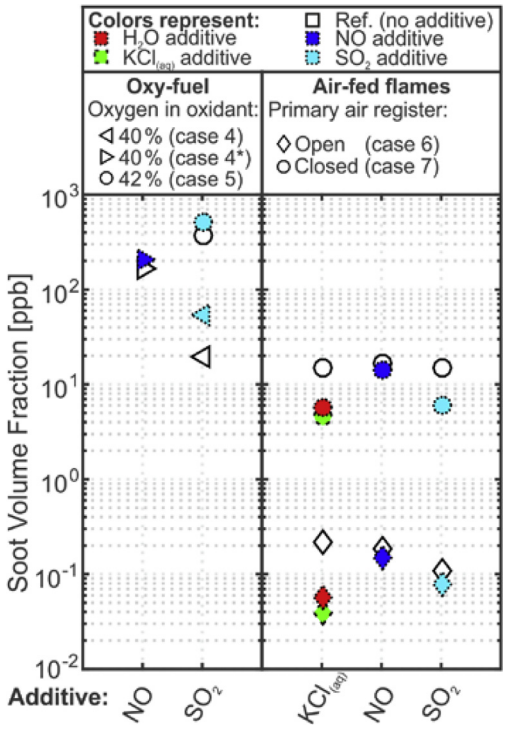

Fig. 5. The effects of different additives ($KCl_{(aq)}$, H_2O, NO, and SO_2) to some of the investigated oxy-fuel and air flame cases. The results have been averaged from calibrated LII images. Case 4* has the same settings as the normal case 4, however, with significant increased soot concentrations probably due to a thermal effect after running the furnace for a full day.

effect for additions of SO_2. Measurements with the KCl-additive could, however, not be evaluated rigorously due to significant KCl-deposits on the windows thereby preventing optical detection.

For the air-fed flame cases 6 and 7, the first observation is that with closed primary air register the soot volume fraction becomes much higher, which can be related to less mixing between air and fuel. Secondly, when comparing the results from oxy-fuel flames (case 4 and 5) with those from the air-fed flame (case 6 and 7) for the additives of NO and SO_2, the effect is opposite, i.e. a decrease of soot volume fraction is observed for the air-fed cases, with a larger decrease for SO_2 addition. Several previous studies have shown lower soot concentrations for additions of SO_2 for different flame types. Lawton studied SO_2 addition to premixed C_2H_4/O_2/argon-flames and observed lower soot concentrations as well as lower PAH-concentrations, and attribute the soot reduction to increased oxidation [25]. Gülder reports lower soot concentrations in sooting diffusion flames when SO_2 is added to the oxidant (air) and attribute the reduction to a thermal effect [26]. Few studies have reported on the impact of NO_x on soot formation. Cotton et al. [27] suggest a mechanism for the soot reduction observed for NO and SO_2-additives, based on catalysis of radical recombination. A recent paper by Abián et al. reports that NO reduces soot concentrations in ethylene pyrolysis experiments in the range 975 −1475 K [28]. They hypothesize that NO interacts with C_2H radicals formed from C_2H_4 leading to CO and HCN. The reason for the increased soot concentration observed for SO_2 and NO additions to the oxy-fuel flames is still unknown.

The largest decrease in soot volume fraction resulted from addition of KCl solution, with the same effect for both open and closed primary oxidant registers. Interestingly, the results show that the largest soot reducing effect in these measurements comes from adding water alone to the flames, and that the additions of $KCl_{(aq)}$ only contributed with a minor additional effect. Hence, this observation indicates that there is a large temperature effect for the decrease in soot concentration when adding the KCl solution. The results from the additives with KCl show the same trend with decreasing soot concentrations as in previous work in small-scale laboratory flames [20,29].

The soot volume fractions from the LII measurements presented in this work are quantitative through in-situ calibration using extinction. The main uncertainties of the soot volume fractions are for the presented cases with low absorption in the furnace (i.e. all cases except case 5, which is discussed later) mainly considered to be the estimation of $E(m)$ and the variation of the probe volume along the beam propagation direction. In this work we selected $E(m) = 0.35$ based on recent measurements in ethylene/air flames [22,23]. The variation of optical properties of soot found in literature is large. In [30], complex refractive indices of soot from different studies are presented, resulting in a variation of $E(m)$ mainly between 0.12 and 0.30. This means that by choosing a specific $E(m)$, large uncertainties will be introduced in the calculation of soot volume fraction as it is inversely proportional to $E(m)$. Another experimental uncertainty comes from the sheet-forming optics for creating the thin laser sheet inside the furnace. Despite using a long focal length cylindrical lens in our setup ($f = 2$ m) leading to a longer beam waist, there exist significant variations in the laser beam thickness for the imaged region with a width of around 15 cm. For cases where measurements are performed on the LII plateau at low soot concentrations, the increased probe volume in the regions far from flame center will lead to relatively stronger LII signals. Still, the averaged soot volume fraction will remain unaffected since it is derived from the extinction measurements.

High concentrations of soot result in several measurement problems. In our study, such conditions are represented by case 5. Firstly, from the averaged image shown in Fig. 4b (second image), it is clear that the signal decreases from right to left (laser beam enters the furnace from the right). This is due to extinction of the laser beam due to very high soot concentrations. For the present case, the transmission through the furnace was measured to 13% at a wavelength of 808 nm. Hence, the laser fluence was gradually reduced along the beam propagation path eventually resulting in fluence below the laser fluence plateau. Secondly, the induced LII signal will, due to the high absorption, also be absorbed when the signal passes from the center of the furnace to the camera. A third problem that was encountered was windows fouling. Even though CO_2 was used for purging the windows for the oxy-fuel cases (air was used for the air-fed cases), they were still to some extent contaminated by the soot inside the furnace. In Fig. 4b (third image) an image is shown after applying a compensation routine based on extinction measurements resulting in a much more even distribution. However, it is clear that despite compensations, the uncertainties for case 5 are much larger than for the more low-sooting cases. One of the additional uncertainties for case 5, was the estimation of absorption length as larger part of the LII signals came from the regions outside the imaged region. In the same image, a striping pattern can be observed, caused by variations in energy in the vertical profile of the laser beam originating from spatial beam inhomogeneity and beam steering effects.

4. Conclusions

Laser-induced incandescence measurements, calibrated using in-situ extinction measurements, have successfully been performed to obtain quantitative information of soot volume fractions, f_v, for 80 kW propane diffusion flames in an oxy-fuel environment. Two-dimensional instantaneous LII images showed highly localized soot regions and turbulent flame structure. The results showed an increasing soot volume fraction for increased oxygen concentrations in the oxidant with constant overall oxygen-to-fuel equivalence ratio. This is most likely an effect of a temperature increase and less mixing due to reduced recirculation of CO_2 inside the furnace. The additives SO_2 and NO resulted in increased in-situ soot volume fractions for oxy-fuel flames, and decreased soot volume fractions for the air-fed cases. For the air-fed cases, the KCl water solution resulted in decreased soot volume fractions, where the main effect was found to come from the water addition. The soot concentration data from the campaign will be used for radiative heat transfer models to be presented elsewhere. The main uncertainties in the quantitative 2-D soot volume fraction data are, for the low-sooting cases, found to be the uncertainty in $E(m)$, and the variation of laser sheet thickness due to the focusing of the laser sheet over a large area in the present experiments. For high-sooting cases, additional uncertainty in f_v arises from the absorption length estimation and extinction of laser beam through the furnace as well as LII signal towards the detector.

Acknowledgments

The authors would like to thank the Swedish Energy Agency through the Swedish Gasifica-

tion Centre (SFC) (34721-2) and through the CECOST incentive program (207) for financial support. This project also acknowledges funding from the EU Horizon 2020 research and innovation programme under the Marie Skłodowska-Curie grant agreement No.675528. Rikard Edland and Thomas Allgurén are also acknowledged for their help during the measurements.

References

[1] T.C. Bond, S.J. Doherty, D.W. Fahey, et al., *J. Geophys. Res. Atmos.* 118 (2013) 5380–5552.
[2] WHO, *Health Aspects of Air Pollution with Particulate Matter, Ozone and Nitrogen Dioxide*, Report No. EUR/03/5042688, Bonn, Germany, 13–15 January, 2003.
[3] IPCC, Contribution of Working Group I to the Fifth Assessment Report of the Intergovernmental Panel on Climate Change, in: T.F. Stocker, D. Qin, G.-K. Plattner, M. Tignor, S.K. Allen, J. Boschung, A. Nauels, Y. Xia, V. Bex, P.M. Midgley (Eds.), *Contribution of Working Group I to the Fifth Assessment Report of the Intergovernmental Panel on Climate Change*, Cambridge University Press, Cambridge, United Kingdom and New York, NY, USA, 2013.
[4] K. Andersson, F. Johnsson, *Fuel* 86 (2007) 656–668.
[5] D. Bäckström, D. Gall, M. Pushp, R. Johansson, K. Andersson, J.B.C. Pettersson, *Exp. Therm. Fluid Sci.* 64 (2015) 70–80.
[6] T. Ekvall, K. Andersson, T. Leffler, M. Berg, *Proc. Combust. Inst.* 36 (2017) 4011–4018.
[7] K. Andersson, R. Johansson, F. Johnsson, B. Leckner, *Energy Fuels* 22 (2008) 1535–1541.
[8] K. Andersson, R. Johansson, S. Hjärtstam, F. Johnsson, B. Leckner, *Exp. Therm. Fluid Sci.* 33 (2008) 67–76.
[9] R.S. Mehta, M.F. Modest, D.C. Haworth, *Combust. Theor. Model.* 14 (2010) 105–124.
[10] D. Bäckström, A. Gunnarsson, D. Gall, X. Pei, R. Johansson, K. Andersson, R.K. Pathak, J.B.C. Pettersson, *Combust. Flame* 186 (2017) 325–334.
[11] C. Schulz, B.F. Kock, M. Hofmann, H. Michelsen, S. Will, B. Bougie, R. Suntz, G. Smallwood, *Appl. Phys. B* 83 (2006) 333–354.
[12] H.A. Michelsen, C. Schulz, G.J. Smallwood, S. Will, *Prog. Energy Combust.* 51 (2015) 2–48.
[13] C.K. Stimpson, A. Fry, T. Blanc, D.R. Tree, *Proc. Combust. Inst.* 34 (2013) 2885–2893.
[14] C.R. Shaddix, T.C. Williams, *Proc. Combust. Inst.* 36 (2017) 4051–4059.
[15] H. Bladh, J. Johnsson, P.-E. Bengtsson, *Appl. Phys. B* 90 (2008) 109–125.
[16] C.F. Bohren, D.R. Huffman, *Absorption and scattering of light by small particles*, Wiley, New York, 1998.
[17] J. Simonsson, N.-E. Olofsson, S. Török, P.-E. Bengtsson, H. Bladh, *Appl. Phys. B* 119 (2015) 657–667.
[18] H. Bladh, P.-E. Bengtsson, *Appl. Phys. B* 78 (2004) 241–248.
[19] N.-E. Olofsson, J. Johnsson, H. Bladh, P.-E. Bengtsson, *Appl. Phys. B* 112 (2013) 333–342.
[20] J. Simonsson, N.-E. Olofsson, H. Bladh, M. Sanati, P.-E. Bengtsson, *Proc. Combust. Inst.* 36 (2017) 853–860.
[21] X. Pei, *A Soot Transformation Study: Interactions Between Soot, Sulfuric Acid and Secondary Organic Aerosol (SOA), Department of Chemical and Molecular Biology, Faculty of Science*, University of Gothenburg, Gothenburg, Sweden, 2018.
[22] H. Bladh, J. Johnsson, N.-E. Olofsson, A. Bohlin, P.-E. Bengtsson, *Proc. Combust. Inst.* 33 (2011) 641–648.
[23] N.-E. Olofsson, J. Simonsson, S. Török, H. Bladh, P.-E. Bengtsson, *Appl. Phys. B* 119 (2015) 669–683.
[24] I. Glassman, *Combustion*, fourth ed., Academic Press, San Diego, 2008.
[25] S.A. Lawton, *Combust. Flame* 75 (1989) 175–181.
[26] Ö.L. Gülder, *Combust. Flame* 92 (1993) 410–418.
[27] D.H. Cotton, N.J. Friswell, D.R. Jenkins, *Combust. Flame* 17 (1971) 87–98.
[28] M. Abián, E. Peribáñez, Á. Millera, R. Bilbao, M.U. Alzueta, *Combust. Flame* 161 (2014) 280–287.
[29] B.S. Haynes, H. Jander, H.G. Wagner, *Proc. Combust. Inst.* 17 (1979) 1365–1374.
[30] T.C. Bond, R.W. Bergstrom, *Aerosol Sci. Technol.* 40 (2006) 27–67.